CrystEngComm

Accepted Manuscript

Journal Name RSCPublishing

ARTICLE

Synthesis, Structure, and Piezoelectric Property of Ferroelectric and Antiferroelectric $NaNbO_3$ Nanostructures

Cite this: DOI: 10.1039/x0xx00000x

Received 00th January 2012,
Accepted 00th January 2012

DOI: 10.1039/x0xx00000x

www.rsc.org/

Shaozheng Ji,[a] Hong Liu,*[ab] Yuanhua Sang,[a] Wei Liu,[a] Guangwei Yu,[a] Yanhua Leng[a]

$NaNbO_3$ cubes and nanowires have been synthesized by hydrothermal based method utilizing thin Nb foil and low concentration NaOH solution with the existence of H_2O_2. $Na_2Nb_2O_6$-H_2O precursor can be obtained under hydrothermal condition at 200°C for only 4 hours. Both long-time hydrothermal treatment and calcination on the precursor nanowires can realize the transition from $Na_2Nb_2O_6$-H_2O nanowires to $NaNbO_3$ crystalline particles. However, the crystalline phase of the two products are different. $NaNbO_3$ microcubes obtained from long-time hydrothermal treatment are antiferroelectric phase with space group Pbma, while $NaNbO_3$ nanowires obtained by annealing $Na_2Nb_2O_6$-H_2O at 500°C for 3 hours are ferroelectric phase with space group $P2_1ma$. The experimental results from X-ray diffraction (XRD), field emission scanning electron microscopy (FESEM), high resolution electron microscopy (HRTEM) and Raman spectroscopy proved the difference of crystalline phase between the $NaNbO_3$ microcubes and nanowires. Piezoelectric force microscope (PFM) detection proved that $NaNbO_3$ nanowires possess piezoelectricity, while no piezoelectric response can be detected for $NaNbO_3$ microcubes synthesized by direct hydrothermal treatment.

Introduction

Alkaline niobates are very important functional materials due to their piezoelectricity, pyroelectricity, electro-optic, photovoltaic effect, nonlinear optical response and photocatalytic properties.[1-5] As one of the important members of this group, sodium niobate ($NaNbO_3$) has attracted great attentions recently because of the exceptional piezoelectric response in $NaNbO_3$-derived ceramics which is a promising lead-free alternative to the wide-used lead-based piezoelectric ceramics $Pb(Zr_xTi_{1-x})O_3$(PZT).[6] $NaNbO_3$ and $NaNbO_3$-derived nanocrystals[7-9] have been widely studied and found applications as photocatalyst[10, 11] and piezoelectric nanogenerator[12]. Furthermore, the polymorphism of $NaNbO_3$ based on its perovskite structure is quite complicated, and for the close relationship between crystalline structure and functional properties, many researchers have studied the influences of temperature, crystal size and other parameters on its crystalline structure.[13-17]

$NaNbO_3$ single crystals and ceramics at room temperature are commonly recognized as an antiferroelectric phase with orthorhombic unit cell, space group Pbma. In a study by Shuvaeva and co-workers[18], $NaNbO_3$ in this antiferroelectric phase can be induced to a ferroelectric phase by a sufficient external electric field. Its unit cell is orthorhombic in the polar space group $P2_1ma$ with parameters: a=5.569Å, b=7.790Å, and c=5.518 Å. Shiratori et al.[19] have reported that the phase transition can also be induced by particle size. Karen E. Johnston et al.[13] compared the solid-state preparation, molten salt preparation and Sol-Gel preparation products, and concluded that synthetic route heavily influences both crystal structure and microstructure.

$NaNbO_3$ powders have been synthesized by traditional solid-state techniques, hydrothermal method, microemulsion-mediated approach, solvothermal method and so on.[20-23] Hydrothermal method has been proved to be simple mild and cost-effective. Nb_2O_5 and high concentration NaOH are generally utilized as the starting reagents.[22, 24] Nb powder[25], $Nb(OC_2H_5)_5$[20] were also chosen as the Nb-source. In this paper, quite thin niobium foil with 0.05mm thickness and low concentration NaOH were chosen as the starting materials. The reaction process and structure evolution under hydrothermal condition were studied in detail. Two kinds of $NaNbO_3$ powders, $NaNbO_3$ microcubes and $NaNbO_3$ nanowires, were obtained based on the hydrothermal process. Because of the polymorphism of $NaNbO_3$, X-ray diffraction and Rietveld refinement were utilized to analyse the crystalline structures of $NaNbO_3$ microcubes and $NaNbO_3$ nanowires. Raman spectroscopy and piezoelectric force microscope (PFM) were used to provide evidences to clarify the difference between these two kinds of $NaNbO_3$. It was found that $NaNbO_3$ microcubes are antiferroelectric phase with space group Pbma, while $NaNbO_3$ nanowires are ferroelectric phase with space group $P2_1ma$. The ferroelectric $NaNbO_3$ nanowires may have applications in future devices such as

data storage memories, energy harvesting devices and electromechanical systems.

Experimental Procedure

Sample preparation

The starting materials, sodium hydroxide (NaOH) and hydrogen peroxide (H_2O_2, 30%), were purchased from Sinopharm Chemical Reagent Co., Ltd, China, which are AR grade without any purification. Metallic niobium foil (Nb, 99.99%) with thickness of 0.05mm was chosen as the Nb-source in this experiment. Nb foil was cleaned in alcohol by sonication for 15 min. $Na_2Nb_2O_6$-H_2O nanowires were firstly prepared by hydrothermal method. In a typical synthesis process, a piece of thin Nb foil (20*10*0.05mm) was placed in the bottom of a Teflon-lined autoclave (capacity, 25ml). 5-17ml 2.0M NaOH solution with 2ml H_2O_2 (30%) was then added into the autoclave. The sealed autoclave was kept in an electric oven for 4h at 200°C. The obtained white precipitation was dispersed in deionized water by ultrasonic treatment for 30min, then rinsed with deionized water for 3 times, and dried at 60°C for overnight. Based on $Na_2Nb_2O_6$-H_2O nanowires, there are two methods to synthesize $NaNbO_3$ particles. One is to prolong the hydrothermal treatment time to transform $Na_2Nb_2O_6$-H_2O into $NaNbO_3$. In order to study the transformation process, the products for hydrothermal treatment 8h, 12h and 24h were all obtained. The other approach is taking $Na_2Nb_2O_6$-H_2O nanowires as precursor, and getting $NaNbO_3$ nanowires by careful calcination. Typically, $NaNbO_3$ nanowires could be obtained by annealing the precursor at 500°C for 3h.

Characterization

Field emission scanning electron microscopy (FESEM, Model JSM-7600F, JEOL Ltd., Tokyo, Japan) was used to characterize the morphology and size of the synthesized samples. High resolution transmission electron microscopy (HRTEM) images were carried out with a JOEL JEM 2100F microscope. X-ray powder diffraction (XRD) patterns were recorded on a Bruker D8 Advance powder X-ray diffractometer with Cu Kα (λ =0.15406 nm). TG/DTA characterization was done on Diamond TG/DTA, Perkin Elmer. Raman spectroscopy was measured on Jobin-Yvon HR 800 with 473nm excitation laser. IR spectra were obtained on a Nicolet FTIR760 infrared spectrometer. Piezoelectric force microscope (PFM) was performed on Bruker Dimension Icon Scanning Probe Microscope using Pt coated conductive tip. In order to measure the piezoelectric property of powder sample, the powders were firstly dispersed in alcohol and then dropped on an Au-coated silicon wafer. The prepared sample was kept in a 200°C electric oven for 2h to fix the powder on the surface of silicon wafer.
Rietveld refinements were carried out on the powder XRD data with the General Structure Analysis System (GSAS) program and EXPGUI front-end [26, 27] using the structural information from the X-ray Powder diffraction data as the starting point. The high intensity XRD data was obtained by slow scan speed (1s/step with step length of 0.02°) from 15° to 120° on Bruker D8 Advance powder X-ray diffractometer. A pseudo-Voigt function (GSAS type#4) was used as the profile function for the XRD datasets. Rietveld refinements of the model in space group $P2_1ma$ and space group Pbma were under taken using the model of Shuvaeva.[18] and Hongwu Xu et.al.[28], respectively.

Results and Discussion

The XRD patterns of the products obtained from hydrothermal treatment at 200°C for 4h-24h are shown in Fig. 1. In Fig. 1(a), all the peaks in the XRD pattern can be indexed as peaks of $Na_2Nb_2O_6$-H_2O. $Na_2Nb_2O_6$-H_2O is the end-member of Sandia octahedral molecular sieves (SOMS) which are a new class of octahedral microporous phases with the compositions $Na_2Nb_{2-x}M_xO_{6-x}(OH)_x\cdot H_2O$(M=Ti,Zr;0<x≤0.4) and possess a framework structure composed of [NbO_6], [MO_6], and [NaO_6] octahedral linked by corner- or edge-sharing.[29-31] When

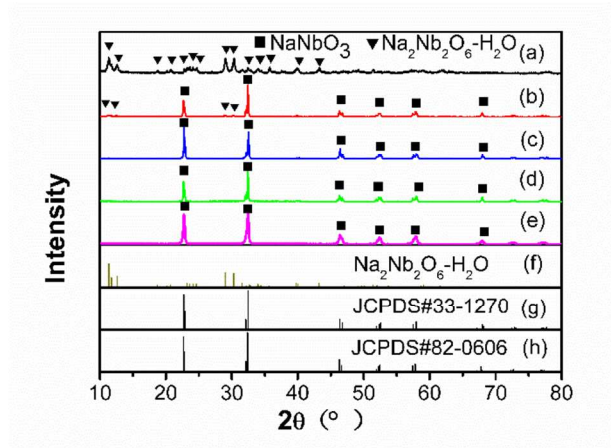

Fig.1 XRD patterns of products at hydrothermal condition for (a)4h,(b)8h,(c)12h,(d)24h and (e) the calcined product obtained by annealing 4h-product at 500℃ for 3h. Pattern (f) is the standard diffraction pattern of $Na_2Nb_2O_6$-H_2O. Pattern (g) and (h) correspond to the standard diffraction pattern of $NaNbO_3$ in Pbma space group and $NaNbO_3$ in $P2_1ma$ space group, respectively.

hydrothermal reaction time was increased to 8h, the XRD pattern in Fig. 1(b) shows that most of the peaks belonging to $Na_2Nb_2O_6$-H_2O disappear except for four small peaks. The new peaks with high intensity can be indexed as the peaks of $NaNbO_3$, which means that $NaNbO_3$ with a good crystallinity is formed. When further prolonging hydrothermal time to 12h, all the peaks can be indexed to $NaNbO_3$ without any of them belonging to $Na_2Nb_2O_6$-H_2O as shown in Fig. 1(c). When increasing hydrothermal time to 24h, the product has no phase change anymore. Pattern (g) and (h) in Fig. 1 show the standard diffraction patterns of $NaNbO_3$ in Pbma (JCPDS#33-1207) and $P2_1ma$ space group (JCPDS#82-0606), respectively. These two diffraction patterns look like the same, making it hard to index the accurate crystalline structure of hydrothermal products. However, from the phase evolution as shown in Fig. 1, it can be concluded that $Na_2Nb_2O_6$-H_2O is metastable under

hydrothermal condition. With hydrothermal time increasing, the precursor molecules lose combined water and convert into $NaNbO_3$. After 12h hydrothermal treatment, pure $NaNbO_3$ can be obtained.

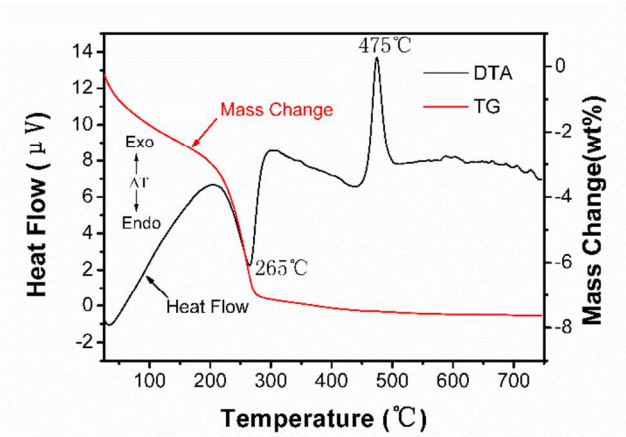

Fig.2 TG/DTA curve of $Na_2Nb_2O_6$-H_2O

TG/DTA measurement on $Na_2Nb_2O_6$-H_2O powder was performed in air from room temperature to 750°C to investigate its stability and predict the phase transition during heating treatment. The obtained curve is shown in Fig.2. There is an endothermic peak at 265°C. The corresponding weight loss is ~4.2%. This is close to the ideal value of 5.2% weight percent of combined water based on the formula $Na_2Nb_2O_6$-H_2O. So the endothermic peak at 265°C is due to the loss of the combined water. An exothermic peak appears at 475°C without weight loss which arises from the transition of $Na_2Nb_2O_6$ to its dense form.[29] When annealing $Na_2Nb_2O_6$-H_2O at 500°C for 3h, the obtained product is $NaNbO_3$ as shown in Fig. 1(e). It can be seen that the product has good crystallographic quality. When annealing $Na_2Nb_2O_6$-H_2O at 300°C or 400°C for 3h, $NaNbO_3$ could not be formed (Fig. S1of the ESI†). This is agreed with the TG/DTA curve of $Na_2Nb_2O_6$-H_2O. When comparing the XRD patterns of $NaNbO_3$ obtained by long time hydrothermal treatment (Fig. 1(d)) with that obtained by annealing $Na_2Nb_2O_6$-H_2O (Fig. 1(e)), no obvious difference could be observed. A detailed discussion will be shown later to confirm their accurate crystalline structures.

IR spectra of hydrothermal products and product obtained by annealing $Na_2Nb_2O_6$-H_2O at 500°C are shown in Fig. 3. In Fig. 3(a), the peak 3207.9cm^{-1} and 3369.1cm^{-1} corresponds to the vibration of O-H. The peak 1696.7cm^{-1} can be attributed to H-O-H bend of the molecular water. The absorption bands below 1000cm^{-1} are vibrations of Na-niobate framework including M-O stretching, M-O-M bending (M= Nb, Na), and lattice vibrations.[30] With the increasing of hydrothermal time, the intensity of the peaks 3207.9cm^{-1}, 3369.1cm^{-1} and 1696.7cm^{-1} decreases till to disappear completely in 24h hydrothermal product. It can be inferred that the water in hydrothermal products decreases gradually till to disappear with the increasing of hydrothermal time. In the range of below 1000 cm^{-1}, the divided adsorption peaks broaden gradually to a wider absorption range with the increasing of hydrothermal time which is corresponded to the phase transition from $Na_2Nb_2O_6$-H_2O to $NaNbO_3$. The IR spectra of 24h hydrothermal product (Fig. 3(d)) and the calcined $NaNbO_3$ product (Fig. 3(e)) are almost the same which means that 24h hydrothermal product are pure $NaNbO_3$ without $Na_2Nb_2O_6$-H_2O. The evolution of IR spectra proves that during hydrothermal process $Na_2Nb_2O_6$-H_2O loses combined water and transfers to $NaNbO_3$ phase ultimately which agrees well with the XRD result.

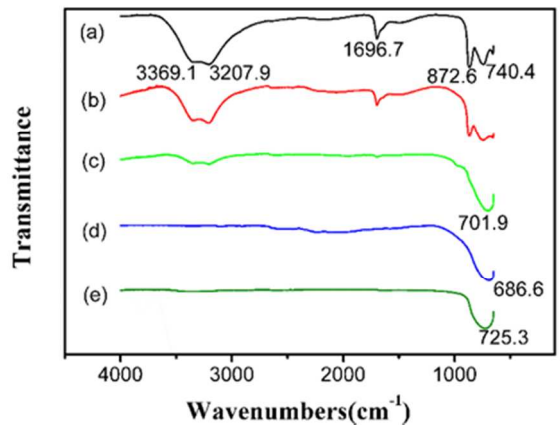

Fig.3 IR spectra of products at hydrothermal condition for (a)4h, (b)8h, (c)12h, (d) 24h and (e) calcined product by annealing 4h product at 500°C for 3h

Morphological observation on the samples of different hydrothermal time and the calcined product obtained by annealing $Na_2Nb_2O_6$-H_2O at 500°C is shown in Fig. 4. The 4h-product is $Na_2Nb_2O_6$-H_2O nanowire with 10-20μm in length and about 150nm in width as shown in Fig. 4(a,b). Delamination at the end of one $Na_2Nb_2O_6$-H_2O nanowire is shown in Fig. 4(c). The boundary coming from different layer at the end is clear which may signify the layer structure of $Na_2Nb_2O_6$-H_2O. The 8h-product shown in Fig. 4(d) is the mixture of micro-sized irregular blocks and nanowires. The surface of blocks is rough covering some nanowires. Fewer nanowires appear in 12h-proudct shown in Fig. 4(e) and micro-sized regular cubes with smooth surface begin to appear. In Fig. 4(f), all the particles synthesized for 24 hours hydrothermal treatment are micro-sized cubes with some cubes cross together, and the surface of cubes is smooth as shown in Fig. 4(g). The transformation mechanism from $Na_2Nb_2O_6$-H_2O nanowires to $NaNbO_3$ cubes can be found in Ref 17. $Na_2Nb_2O_6$-H_2O dissolves to provide the source of [NbO_6] or clusters of [NbO_6] for the growth of the $NaNbO_3$ cubes. FESEM and HRTEM images of the calcined product by annealing $Na_2Nb_2O_6$-H_2O precursor at 500°C for 3h are shown in Fig. 4(h) and Fig. 4(i,j), respectively. The calcined $NaNbO_3$ basically keeps the nanowire morphology with about 50nm in width as shown in Fig. 4(i). The lattice structure of calcined $NaNbO_3$ is shown in Fig. 4(j). $NaNbO_3$ nanowire has a high crystalline quality evidenced by clear lattice fringes. The interplanar spacing is 0.389nm and 0.392nm in two perpendicular directions. The inset in Fig. 4(j) is the fast

Fourier transform (FFT) image of $NaNbO_3$ which shows its orthorhombic crystalline structure.

As mentioned above, $NaNbO_3$ nanowires obtained by annealing $Na_2Nb_2O_6$-H_2O precursor, and $NaNbO_3$ microcubes synthesized by prolonging the hydrothermal treatment time may be different in crystalline structure. To recognize the difference of crystalline structure between the two products, XRD patterns with high intensity on the two samples were got, and the lattice parameters were obtained by Rietveld refinements. In Fig.1, the XRD patterns of product powder synthesized at hydrothermal condition for 24 hours and product obtained by annealing $Na_2Nb_2O_6$-H_2O precursor look like the same. However, if we enlarge the XRD patterns, there are some obvious differences

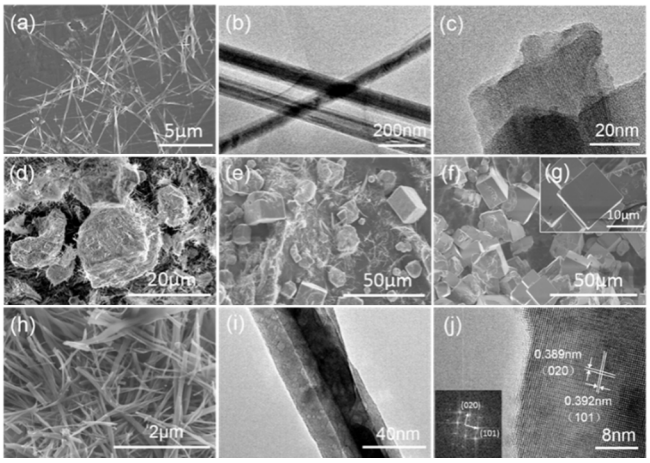

which are shown in Fig. 5. In the range of 31°-33°and 45.5°-47.5°, there are two diffraction peaks both for $NaNbO_3$

Fig.4 (a)SEM image of $Na_2Nb_2O_6$-H_2O obtained by 4h hydrothermal treatment. (b),(c) HRTEM images of $Na_2Nb_2O_6$-H_2O nanowire. Images(d),(e),(f) are SEM images of 8h,12h and 24h hydrothermal treatment products, respectively. Image (g) is the partial enlargement of image(f). Image(h) is SEM image of product obtained by annealing $Na_2Nb_2O_6$-H_2O precursor nanowires. Image (i) and (j) are the HRTEM images of product synthesized by annealing $Na_2Nb_2O_6$-H_2O precursor nanowires. The inset in image(j) is fast Fourier transform (FFT) pattern for $NaNbO_3$.

synthesized by 24h hydrothermal treatment and that by annealing $Na_2Nb_2O_6$-H_2O precursor, which agreed well with two standard JCPDS cards No. 33-1270 (Pbma) and No. 86-0606($P2_1ma$), respectively. In the range of 35.5°-37.5°, there are three peaks in $NaNbO_3$ synthesized by 24h hydrothermal treatment while there are only two peaks in $NaNbO_3$ obtained by annealing $Na_2Nb_2O_6$-H_2O precursor which also agreed with the two JCPDS cards. In the range of 54°-56°, $NaNbO_3$ synthesized by 24h hydrothermal treatment has diffraction peak while that obtained by annealing $Na_2Nb_2O_6$-H_2O precursor doesn't have. From these features, $NaNbO_3$ synthesized by 24h hydrothermal treatment can be indexed to JCPDS No.33-1270 (Pbma) while $NaNbO_3$ obtained by annealing $Na_2Nb_2O_6$-H_2O precursor can be indexed to JCPDS No.86-0606($P2_1ma$). The former is an antiferroelectric phase and the latter is a ferroelectric structure. In order to further confirm their phase structure, Rietveld refinements for $NaNbO_3$ synthesized by 24h hydrothermal treatment and $NaNbO_3$ obtained by annealing $Na_2Nb_2O_6$-H_2O precursor were carried out based on the structure of JCPDS No.33-1270 and No.86-0606, respectively. The refinement results are shown in Fig. 6, showing an excellent agreement between observed and calculated patterns. The inset in Fig. 6(a) and Fig. 6(b) are the unit cells of $NaNbO_3$ in Pbma and $P2_1ma$, respectively. Unit cell of Pbma $NaNbO_3$ in Fig. 6(a) displays an unusual "octahedral tilting" scheme with three independent tilts leading to a $\sqrt{2}a_p\times\sqrt{2}a_p\times4a_p$ supercell of the basic cubic perovskite subcell, where a_p is the idealized cubic perovskite lattice parameter. Compared with Pbma $NaNbO_3$, $NaNbO_3$ in $P2_1ma$ possesses a smaller unit cell described by $\sqrt{2}a_p\times\sqrt{2}a_p\times2a_p$ as shown in the inset of Fig. 6(b).[13] In contrast to $NaNbO_3$ in Pbma, the lack of b slip in $P2_1ma$ makes it a noncentrosymmetrical phase and possessing a spontaneous polarization which is the necessary condition for piezoelectric and ferroelectric property. The refined unit cell parameters and atom corporation are listed in Table S1 and S2 of the ESI†. The interplanar spacing 0.389nm and 0.392nm in Fig. 4(j) are corresponded to the crystal plane (020) and (101) of $NaNbO_3$ in $P2_1ma$, respectively.

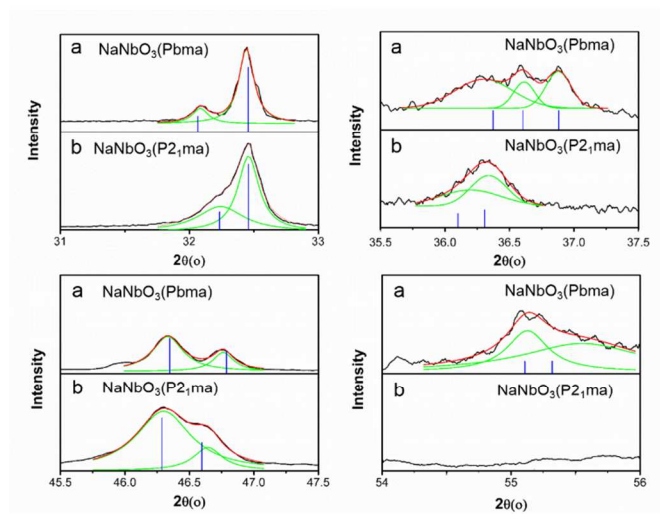

Fig.5 a: XRD patterns of $NaNbO_3$ synthesized by 24h hydrothermal treatment.b: XRD patterns of $NaNbO_3$ obtained by annealing $Na_2Nb_2O_6$-H_2O precursor. The four images show the difference of their XRD patterns in the range of 31°-33°, 35.5°-37.5°, 45.5°-47.5°, 54°-56°. The blue lines show the position and relative intensity of the standard diffraction peaks.

Raman spectroscopy is sensitive to the octahedral tilting associated with the $NaNbO_3$ phase structure. Therefore, Raman spectra were recorded to further prove the difference of these two samples under 473nm laser excitation. The obtained Raman spectra are shown in Fig. 7. A remarkable difference between Fig. 7(a) and Fig. 7(b) can be observed within the region between 150cm^{-1} to 300cm^{-1}, as shown in the insets of Fig.7(a) and (b). In this range, spectrum in Fig. 7(a) shows obvious splitting peaks compared with spectrum in Fig. 7(b).

The peak at 219cm^{-1} in Fig. 7(a) almost disappears in Fig. 7(b) and the location of highest peak has a small shift. All the bands in the range 150–1000 cm^{-1} are associated with the internal vibrational modes of NbO_6. The region from 150 to 300 cm^{-1} is related to the triply degenerate v_6 (F2u) and v_5 (F2g) modes.[15, 20] The spectrum of $NaNbO_3$ obtained by annealing $Na_2Nb_2O_6$-H_2O precursor agrees well with the $P2_1ma$ phase reported in reference 14. Raman spectroscopy further proved the structural difference of $NaNbO_3$ synthesized by 24h hydrothermal treatment and by annealing $Na_2Nb_2O_6$-H_2O precursor.

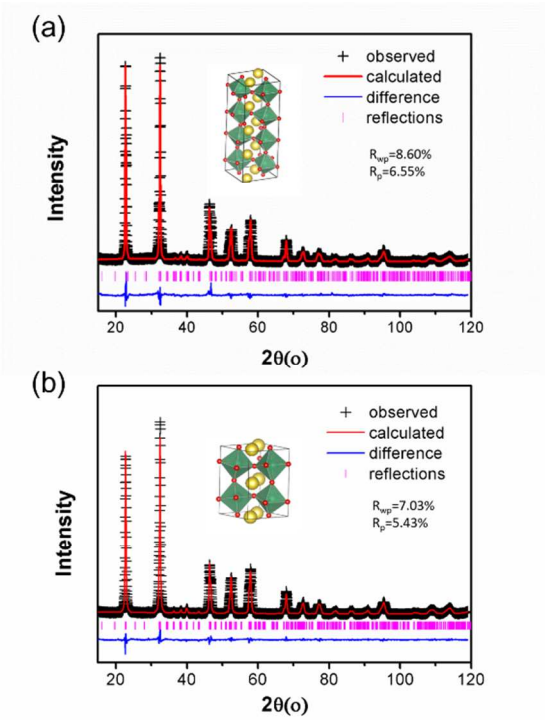

Fig.6 Fitted XRD patterns of (a) $NaNbO_3$ synthesized by 24h hydrothermal treatment and (b) $NaNbO_3$ obtained by annealing $Na_2Nb_2O_6$-H_2O precursor. Plus (+) symbols represent the measured results and the solid line is from refinement. The difference between observed and calculated results is shown beneath (blue). The insets in Fig. 6(a) and Fig. 6(b) are the unit cells of $NaNbO_3$ in Pbma symmetry and $P2_1ma$ symmetry, respectively. Yellow and red balls represent Na and O atoms, respectively. The green octahedral represents [NbO_6] unit.

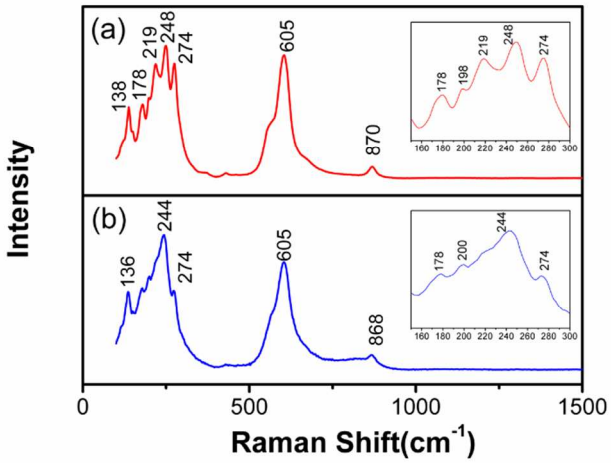

Fig.7 Raman spectra of (a) $NaNbO_3$ synthesized by 24h hydrothermal treatment and (b) $NaNbO_3$ obtained by annealing $Na_2Nb_2O_6$-H_2O precursor. The insets are the enlarged parts from150cm^{-1} to 300cm^{-1}

As is well known, only noncentrosymmetrical crystal structure can possess piezoelectric property. So $NaNbO_3$ nanowires obtained by annealing $Na_2Nb_2O_6$-H_2O precursor with noncentrosymmetrical crystal structure can possess piezoelectric property in theory, while $NaNbO_3$ microcubes synthesized by 24h hydrothermal treatment don't have. Piezoelectric force microscope (PFM) is a common technique for the study of ferroelectric and piezoelectric phenomena in low dimensional materials.[32-34] Therefore, in this work, piezoelectric response of the two samples were characterized by PFM technique. When applying 10V AC voltage on the conductive tip of PFM, the piezoelectric response of $NaNbO_3$ nanowire obtained by annealing $Na_2Nb_2O_6$-H_2O precursor is shown in Fig. 8. Fig. 8(a) depicts the height image for a single $NaNbO_3$ nanowire. Fig. 8(b) and 8(c) show the amplitude and phase maps of the piezoelectric response, respectively. The amplitude and phase images agree well with each other. In Ref. 20, Tsung-Ying Ke et al. also observed the piezoelectric property of $NaNbO_3$ nanowire. The piezoelectric property of $NaNbO_3$ nanowire obtained by annealing $Na_2Nb_2O_6$-H_2O precursor further confirm its noncentrosymmetrical crystal structure. Furthermore, when applying a ramp voltage loop from -10 to 10V and then reversed to the dashed rectangular

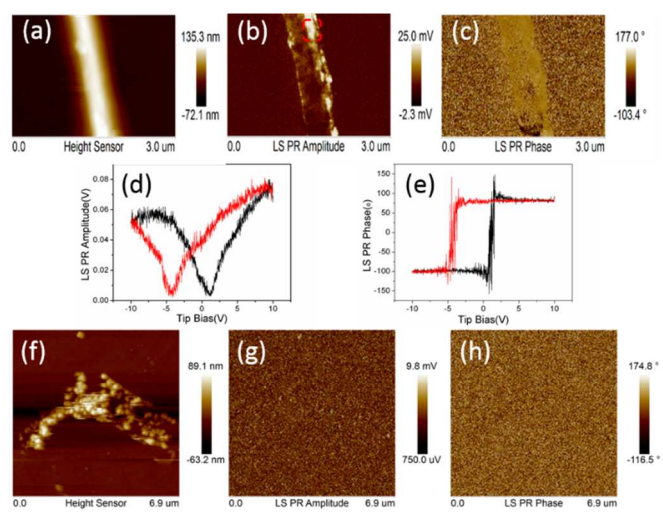

Fig. 8 (a) Height image of a $NaNbO_3$ nanowire obtained by annealing $Na_2Nb_2O_6$-H_2O precursor. (b) The relative amplitude of piezoelectric response and (c) phase of piezoelectric response. When applying ramp voltage from -10 to 10V and then reversed to the dashed rectangular region in ampitude image(b), the standard ferroelectric amplitude curve(d) and phase curve(e) were obtained.(f) is the height image of $NaNbO_3$ powder obtained by 24h hydrothermal treatment. (e) The relative amplitude of piezoelectric response and (f) phase of piezoelectric response.

region in Fig. 8(b), the standard ferroelectric butterfly amplitude curve (Fig. 8(d)) and phase curve (Fig. 8(e)) were obtained. This is the most important evidence that $NaNbO_3$ nanowire possesses typical ferroelectric property. For $NaNbO_3$ microcubes synthesized by 24h hydrothermal treatment, PFM was also used to detect its piezoelectric property. As mentioned in former part, the size of $NaNbO_3$ microcubes is too large to measure the piezoelectric property on PFM. To realize the PFM measurement, the $NaNbO_3$ cubes were grinded to smaller particles, dispersed with ethanol, and fixed on an Au-coated silicon wafer using the procedure described in experimental part. The SEM image with morphology of ground particles is shown in Fig. S2 of the ESI†. The average size of the particles is about 300nm. On the same experimental condition, there is no piezoelectric response observed as shown in Fig. 8(g) and (h), which agrees with its centrosymmetric crystalline structure.

Conclusions

In summary, we have successfully and efficiently synthesized $Na_2Nb_2O_6$-H_2O nanowires by hydrothermal method utilizing thin Nb foil as Nb-source at low concentration of NaOH solution with the existence of H_2O_2. When prolonging hydrothermal treatment time on the same hydrothermal condition, $Na_2Nb_2O_6$-H_2O can lose combined water and then transfer into $NaNbO_3$ microcubes ultimately. $NaNbO_3$ nanowires can be obtained by annealing $Na_2Nb_2O_6$-H_2O nanowires at 500°C. $NaNbO_3$ microcubes and $NaNbO_3$ nanowires have different crystalline structure corresponding to an antiferroelectric crystal structure with Pbma space group and a ferroelectric phase with $P2_1ma$ space group, respectively. Because of the noncentrosymmetrical crystalline structure, $NaNbO_3$ nanowires possessing piezoelectric property may be applied for data storage memories, energy harvesting devices and nanoelectromechanical systems.

Acknowledgements

This research was supported by Natural Science Foundation of China (Grant No.51372142, 21071090), National Science Fund for Distinguished Young Scholars (NSFDYS: 50925205), Innovation Research Group (IRG: 51321091) and the "100 Talents Program" of the Chinese Academy of Sciences.

Notes and references

[a]State Key Laboratory of Crystal Materials, Shandong University, 27 Shandanan Road, Jinan, 250100, China. E-mail: hongliu@sdu.edu.cn,
[b]Beijing Institute of Nanoenergy and Nanosystems, Chinese Academy of Science, Beijing 100864, P. R. China

† Electronic Supplementary Information (ESI) available: [details of any supplementary information available should be included here]. See DOI: 10.1039/b000000x/

1. Y. Nakayama, P. J. Pauzauskie, A. Radenovic, R. M. Onorato, R. J. Saykally, J. Liphardt and P. Yang, *Nature*, 2007, **447**, 1098-1101.
2. F. Dutto, C. Raillon, K. Schenk and A. Radenovic, *Nano. Lett.*, 2011, **11**, 2517-2521.
3. M. Nyman, F. Bonhomme, T. M. Alam, M. A. Rodriguez, B. R. Cherry, J. L. Krumhansl, T. M. Nenoff and A. M. Sattler, *Science*, 2002, **297**, 996-998.
4. Q. P. Ding, Y. P. Yuan, X. Xiong, R. P. Li, H. B. Huang, Z. S. Li, T. Yu, Z. G. Zou and S. G. Yang, *J.Phys.Chem.C*, 2008, **112**, 18846-18848.
5. I. Grinberg, D. V. West, M. Torres, G. Gou, D. M. Stein, L. Wu, G. Chen, E. M. Gallo, A. R. Akbashev, P. K. Davies, J. E. Spanier and A. M. Rappe, *Nature*, 2013, **503**, 509-512.
6. E. Cross, *Nature*, 2004, **432**, 24-25.
7. L. Q. Cheng, K. Wang, Q. Yu and J. F. Li, *J. Mater. Chem. C*, 2014, **2**, 1519-1524.
8. Y. Xu, Q. Yu and J. F. Li, *J. Mater. Chem.*, 2012, **22**, 23221-23226.
9. Z. Wang, H. S. Gu, Y. M. Hu, K. Yang, M. Z. Hu, D. Zhou and J. G. Guan, *CrystEngComm*, 2010, **12**, 3157-3162.
10. K. Saito and A. Kudo, *Inorg. Chem.*, 2010, **49**, 2017-2019.
11. P. Li, S. Ouyang, Y. J. Zhang, T. Kako and J. H. Ye, *J. Mater. Chem. A*, 2013, **1**, 1185-1191.
12. J. H. Jung, M. Lee, J.-I. Hong, Y. Ding, C.-Y. Chen, L.-J. Chou and Z. L. Wang, *Acs Nano*, 2011, **5**, 10041-10046.
13. K. E. Johnston, C. C. Tang, J. E. Parker, K. S. Knight, P. Lightfoot and S. E. Ashbrook, *J.Am.Chem.Soc.*, 2010, **132**, 8732-8746.
14. S. K. Mishra, R. Mittal, V. Y. Pomjakushin and S. L. Chaplot, *Phys. Rev. B*, 2011, **83**, 134105.
15. Z. X. Shen, X. B. Wang, M. H. Kuok and S. H. Tang, *J. Raman. Spectrosc.*, 1998, **29**, 379-384.
16. K. K. Mishra, V. Sivasubramanian and A. K. Arora, *J. Raman. Spectrosc.*, 2011, **42**, 517-521.
17. S. K. Mishra, M. K. Gupta, R. Mittal, S. L. Chaplot and T. Hansen, *Appl. Phys. Lett.*, 2012, **101**, 242907.
18. V. A. Shuvaeva, M. Y. Antipin, R. S. V. Lindeman, O. E. Fesenko, V. G. Smotrakov and Y. T. Struchkov, *Ferroelectrics*, 1993, **141**, 307-311.
19. Y. Shiratori, A. Magrez, W. Fischer, C. Pithan and R. Waser, *J.Phys.Chem.C*, 2007, **111**, 18493-18502.
20. Y. Shiratori, A. Magrez, J. Dornseiffer, F.-H. Haegel, C. Pithan and R. Waser, *J.Phys.Chem.B*, **109**, 20122-20130.
21. J. Koruza, J. Tellier, B. Malič, V. Bobnar and M. Kosec, *J. Appl. Phys.*, 2010, **108**, 113509.
22. H. Y. Zhu, Z. F. Zheng, X. P. Gao, Y. N. Huang, Z. M. Yan, J. Zou, H. M. Yin, Q. D. Zou, S. H. Kable, J. C. Zhao, Y. F. Xi, W. N. Martens and R. L. Frost, *J.Am.Chem.Soc.*, 2006, **128**, 2373-2384.
23. Q. L. Gu, K. J. Zhu, J. S. Liu, P. C. Liu, Y. Cao and J. H. Qiu, *RSC. Adv.*, 2014, **4**, 15104-15110.
24. T. Y. Ke, H. A. Chen, H. S. Sheu, J. W. Yeh, H. N. Lin, C. Y. Lee and H. T. Chiu|, *J.Phys.Chem.C*, 2008, **112**, 8827-8831.
25. L. Liu, B. Li, D. H. Yu, Y. M. Cui, X. F. Zhou and W. P. Ding, *Chem Commun (Camb)*, 2010, **46**, 427-429.
26. A. C. Larson and R. B. V. Dreele, *Los Alamos National Laboratory Report LAUR*, 1994, 86.
27. B. Toby, *J. Appl. Crystallogr.*, 2001, **34**, 210-213.
28. H. W. Xu, Y. L. Su, M. L. Balmer and A. Navrotsky, *Chem. Mater.*, 2003, **15**, 1872-1878.

29. H. W. Xu, M. Nyman, T. M. Nenoff and A. Navrotsky, *Chem.Mater.*, 2004, **16**, 2034-2040.
30. M. Nyman, A. Tripathi, J. B. Parise, R. S. Maxwell and T. M. Nenoff, *J.Am.Chem.Soc.*, 2002, **124**, 1704-1713.
31. M. Nyman, A. Tripathi, H. B. Parise, R. S.Maxwell, W. T. A. Harrison and T. M.Nenoff, *J.Am.Chem.Soc.*, 2001, 1529-1530.
32. A. Gruverman, D. Wu and J. Scott, *Phys. Rev. Lett.*, 2008, **100**, 097601.
33. G. Suyal, E. Colla, R. Gysel, M. Cantoni and N. Setter, *Nano. Lett.*, 2004, **4**, 1339-1342.
34. M. H. Zhao, Z. L. Wang and S. X. Mao, *Nano. Lett.*, 2004, **4**, 587-590.

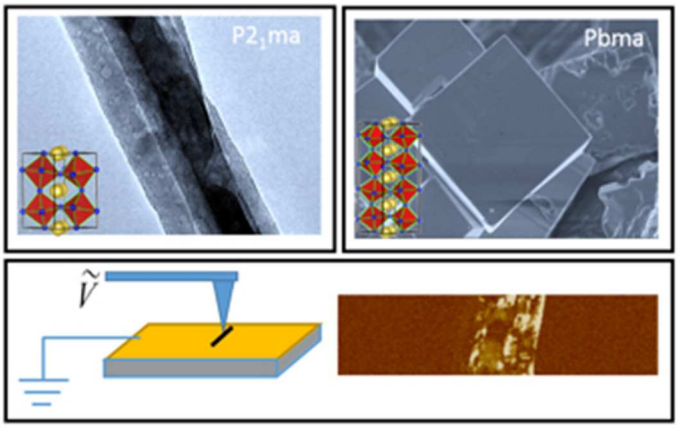

NaNbO3 nanowires and NaNbO3 microcubes are indexed to ferroelectric and antiferroelecric structure, respectively.
59x38mm (150 x 150 DPI)